# Aerial Base Station Assisted Cellular Communication: Performance and Trade-off

Navuday Sharma, Atul Kumar, Haris Pervaiz, Maurizio Magarini, Leila Musavian, Muhamamd Mahtab Alam, Anish Jindal and Muhammad Ali Imran

***Abstract*—The use of Aerial Base Stations (ABSs) has received a great deal of attention in academia and industry as a means to support the cellular communication traffic growth. In this article, we focus on obtaining the optimal altitude of an ABS using two criteria - maximum cell coverage area and minimum Symbol Error Rate (SER). Our study is done by using a probabilistic air-to-ground channel model, developed for low altitude aerial platforms via simulations on a commercial ray tracing software, for different scenarios like Urban High Rise, Urban, and Sub-urban. The probability distributions of the received power of the ground users and of the power delay profile at optimal ABS altitude are provided as a function of the size of the cell area. For the SER analysis, we present a system model based on Generalized Frequency Division Multiplexing (GFDM), in a time-frequency grid that is compatible with Long Term Evolution, by implementing parameters for low latency communication at the physical layer. The impact of "Better than Nyquist" pulses on the GFDM system is evaluated in terms of SER performance. From the presented results, a significant improvement is demonstrated compared to the traditional Nyquist pulses.**

***Index Terms*—Aerial Base Station, Generalized Frequency Division Multiplexing (GFDM), Air-to-Ground channel, Symbol Error Rate (SER), Optimal Altitude, Pulse shaping filters.**

## I. Introduction

THE unmanned aerial vehicles (UAVs[1]), commonly known as drones, have received a rapid proliferation in various applications due to their progress in payload capacity and prolonged battery life [2]. With initial development for military applications, such as surveillance and reconnaissance, UAVs have been also extended to civil sectors such as remote sensing, search and rescue, film making, weather detection, wildlife, agriculture monitoring and smart/secure lockdown monitoring in pandemic [3], [4]. Due to the recent advances in wireless communications, UAVs with low-cost transceivers mounted on board are envisioned to reform the paradigm of next generation networks [5], operating as low altitude aerial base stations (ABSs) and integrated with current cellular architecture [6], as shown in Fig. 1. An ABS can provide on-demand cellular coverage and enhanced data rates to the ground mobile users in a heterogeneous network (HetNet). In this regards, the third generation partnership group (3GPP) provided a technical report, entitled, "Enhanced LTE support for aerial vehicles" in September 2019 with four crucial requirements, as discussed with detail in [7]; listed as UAV traffic requirements; channel modeling to characterize air-to-ground (A2G) propagation; possibility to reuse the current LTE framework for aerial vehicles; and definition of enhancements in LTE Release 17 to assist UAV network. An overview of UAV-aided wireless communications, with three use cases: UAV-aided coverage, UAV-aided relaying, and UAV-aided information dissemination is provided in [8], [9]. Further, such architectures are optimized for enhancing the UAVs performance with respect to various quality-of-service (QoS) parameters such as UAV positioning, cellular coverage, energy optimization, cooperative communication, and routing protocols.

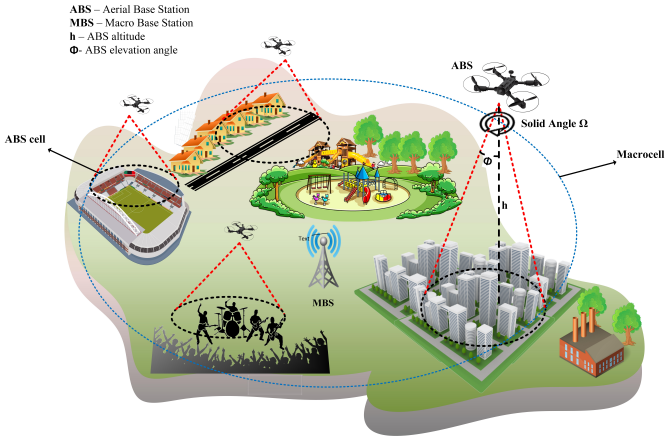


Fig. 1. Wireless cellular network architecture with integrated aerial base stations (ABSs).

The ABS network architecture has a lot of research literature and experimental measurements available for channel characterization, power consumption analysis, placement and mobility optimization, fronthauling and backhauling etc. Here, we address the relevant literature on the aspects of UAV channel modeling, cellular coverage, and waveform analysis based on our motivation and contributions, provided later in this section. Many researchers have presented different methods to tackle some of these issues, as discussed in the following section.

N Sharma **(Corresponding Author)** is with Ericsson Eesti AS, Estonia. A. Kumar is with Vodafone Chair Mobile Communications Systems, Technische Universitat Dresden, Germany. H. Pervaiz is with the School of Computing and Communications (SCC), Lancaster University, UK. M. Magarini is with the Dipartimento di Elettronica, Informazione e Bioingegneria, Politecnico di Milano, Italy. L. Musavian and A. Jindal are with the School of Computer Science and Electronic Engineering, University of Essex, UK. M. M. Alam is with Thomas Johann Seebeck Department of Electronics, Tallinn University of Technology, Estonia, Email: . M. A. Imran is with the School of Engineering, University of Glasgow, UK. Email: navuday.sharma@ericsson.com,atul.kumar@tu-dresden.de, h.b.pervaiz@lancaster.ac.uk, maurizio.magarini@polimi.it, {leila.musavian, a.jindal}@essex.ac.uk, muhammad.alam@taltech.ee, muhammad.imran@glasgow.ac.uk

*The preliminary version of this research work is published in [1].

[1]The term ABS and UAV are used interchangeably through out the article.

### A. Motivation

Despite the vast literature, to the best of our knowledge, there are no articles that consider the generalized waveforms and evaluate their impact on UAV-enabled communication to support low latency and high data rate requirements of ground mobile users, apart from our previous contribution in [1]. In the latter, the symbol-error-rate (SER) analysis was conducted for Generalized Frequency Division Multiplexing (GFDM) based A2G communication with variation of UAV altitude and "Better than Nyquist" (BTN) pulse shaping filters in urban high rise, urban, and suburban environments. In the present article, we further supplement our contribution by adding mobility to the UAV and obtaining an optimal UAV altitude under minimum SER. Also, we evaluate GFDM and OFDM SER for static and moving ABS under various Nyquist and BTN pulse shaping filters.

### B. Relevant Works

A comprehensive survey on channel characterization and modeling for UAV communications, with deterministic and stochastic approaches and measurement campaigns, is provided in [10], as a low altitude aerial platform (LAP). The results of measurement campaigns are described for narrow and wide-band channel sounders, IEEE 802.11 transceivers, and cellular connected UAVs operating at either unlicensed frequency bands or respective bands, according to the considered technology. Furthermore, measurement results are shown for A2G and air-to-air (A2A) characterization with large scale parameters (LSP), such as path loss and shadowing, and small scale parameters (SSP), such as angular spread, delay spreads, and Ricean factor. With focus on similar aspects, reference [11] describes A2A and A2G aeronautical and UAV channel fading statistics, where aeronautical channels suggest the flight altitude of the aircraft is much higher as compared with that of the UAV considered as an LAP. Furthermore, classification of UAVs, timeline of civil aircrafts and UAV channel modeling campaigns are provided along with link budget, channel impulse response, antenna diversity, spatial multiplexing, and multiple-input-multiple-output (MIMO) characteristics over rural, urban, and over the sea environments. Another relevant survey is [12], which describes in detail the impact of the Doppler effect and of the multipath channel propagation in different types of environments. Further, antenna configurations, channel sounding waveforms, effects of elevation angles are extensively elaborated. Since A2G and A2A channels are highly sensitive to line-of-sight (LoS) transmission, the elevation angle plays a significant role in defining the path loss dependence between the transmitter and the receiver. As the impact of elevation angle varies with the antenna directivity, in case of highly directional antennas, such as those used for communications at millimeter waves, the alignment of transmitter and receiver beams has negligible effect on communication for varying elevation angle. However, for omnidirectional or isotropic antennas the effect of the elevation angle can be significant [12], [13]. In [14], the ABS network employs both ultra-high frequency (UHF) and S-bands to provide connectivity to ground users, thus combining the advantages of small path loss in low frequency bands with that of large bandwidth in high frequency bands. Measurements results conducted in rural, suburban, and urban areas are shown with horizontal distance up to $70\,\mathrm{Km}$ from the airship and altitude up to $950\,\mathrm{m}$. Similarly, [15] reports measurements carried out at $3.9\,\mathrm{GHz}$ in suburban environment with an omnidirectional antenna installed on a small UAV flying at an altitude of $40\,\mathrm{m}$. The results of LSP and SSP from the measurements show reasonable agreement when compared with ray tracing simulations for the same scenario. There are several MIMO based UAV channel models, which can be found in [10]–[12]. However, UAV-MIMO channel is out of the scope of this paper.

The literature on UAV cellular coverage is broadly categorized into optimization of various parameters of architectures with single or multiple ABSs. However, there are limited contributions with respect to single ABS coverage. In [16], an analytical analysis is done to maximize the ABS coverage with an optimal altitude, which is a function of path loss and statistical parameters of the urban environment. An LoS path loss model is also derived from the ITU-R mathematical steps, which is used in this paper. In [17], the optimal UAV altitude to establish a reliable maximum coverage is addressed using A2G cooperative communication. Further under a specific scenario with low transmit power, an optimal altitude of $1300\,\mathrm{m}$ is shown without relaying, which varies between $700\,\mathrm{m}$ to $2000\,\mathrm{m}$ with relaying. In [18] the UAV flying altitude and the antenna beamwidth are jointly optimized for throughput maximization for downlink multicasting, broadcasting, and uplink multiple access multiuser communication models. Similarly, the joint optimization of UAV altitude, user association, and transmission direction to improve the system sum-rate with prior knowledge of ground users' location is addressed in [19]. Also, there are many articles proposing an optimal deployment strategy of multiple UAVs' network to maximize the cellular coverage, with the constraints on downlink coverage probability, UAV placement, and minimum transmit power by each UAV. However, we do not refer to those articles in the present paper since we analyze the parameters of a single ABS.

The research on PHY information transmission in ABS is limited. Reference [20], provides the candidate waveforms considering different operating requirements for UAV such as use of control and non-payload communication channel during high altitude cruise, taxing and take-off. Further, it also addresses constraints on UAV size, weight, and power. However, unlike this work, appropriate A2G channel models are not used and the UAV altitude is not taken into account by the authors, thereby discouraging the implementation of new waveforms for information transmission. Also in [21], the authors analyze the growth of UAV industry and spectrum requirements and discuss spectrum sharing as a possible solution to integrate the UAV network into the current cellular infrastructure. They use orthogonal frequency division multiplexing (OFDM) as the most suitable waveform. However, they only consider LoS A2G links in the channel model and ignore the multipath propagation effects, which are included in our simulation results in the range of the same UAV altitudes. In [22], the

TABLE I
SUMMARY OF SYMBOLS AND THEIR DESCRIPTIONS.

| Symbols | Descriptions | Symbols | Descriptions |
|---|---|---|---|
| $\mathbf{d}$ | Vector of high data-rate stream. | $\mathbf{h}$ | Channel impulse response vector of size Sx1. |
| $N$ | Total number of symbols. | $\mathbf{H}$ | Circulant matrix of size SxS based on $\mathbf{h}$. |
| $K$ | Total number of sub-carriers. | $\mathbf{w}$ | Noise vector of size Sx1. |
| $M$ | Total number of sub-symbols. | $\boldsymbol{y}_{eq}$ | Equalized signal in time-domain. |
| $(\cdot)^T$ | Transpose operator. | $\boldsymbol{B}_{MF}$ | Modulator matrix of matched filter. |
| $d_{k,m}$ | $m^{th}$ complex sub-symbol transmitted on $k^{th}$ sub-carrier of the block. | $\mathbf{A}$ | Vector for pulse shaping filter. |
| $T_s$ | Duration of the sub-symbol. | $\hat{d}$ | Estimated data vector. |
| $g_{k,m}[n]$ | Pulse shaping filter. | $\Delta$ | Roll-off factor of pulse shaping filter. |
| $g[n]$ | Prototype filter. | *sech* | Hyperbolic secant function. |
| $\mod$ | modulo $N$ operation. | *arcsech* | Inverse hyperbolic secant function. |
| $N_{CP}$ | Length of the cyclic prefix. | $h$ | Height of ABS. |
| $\eta$ | Path loss exponent. | $R$ | Radius of an area used for normalizing ABS cell area. |
| $\varphi$ | Distance between ground receiver and ABS. | *erf* | Error function. |
| $\varphi_0$ | Reference distance. | $P_{th}$ | Received power threshold of ground users to maintain ABS link connectivity. |
| $X_\sigma$ | Log-normal shadowing. | $P_{TX}$ | Transmitted power by ABS. |
| $\sigma$ | Standard deviation on log-normal shadowing. | $G_T$ | Gain of ABS transmitting antenna. |
| $\mathrm{PL_{LoS}}$ | Path loss of line-of-sight link. | $G_R$ | Gain of users receiving antenna. |
| $\mathrm{PL_{NLoS}}$ | Path loss of non-line-of-sight link. | $\mathrm{PL}_0$ | Reference path loss at distance $r_0$ from the ABS. |
| PL | Average Path loss from LoS and NLoS link. | $\Omega$ | Solid angle. |
| $\mathbb{P}_{\mathrm{LoS}}$ | Probability of LoS link. | $\mathbf{d}$ | 3D distance or the slant height formed from the geometry. |
| $\omega$ and $\varepsilon$ | Parameters of the LoS curve from [16]. | $A$ | Cell area covered by ABS. |
| $\alpha$, $\beta$ and $\gamma$ | Environment structuring variables as described in Sec. IV. | $\hat{n}$ | Unit vector. |
| $\phi$ | Elevation angle between ABS and ground user. | $\theta$ | Azimuth angle between ABS and ground user. |
| $h[n]$ | Channel impulse response. | $P_{RX}$ | Received power by the ground user. |
| $h_\upsilon$ | $\upsilon^{th}$ complex Ricean fading coefficient. | $P_{th}$ | Threshold of received power. |
| $\mathbf{x}$ | Vector of transmitted signal. | $\mathbf{r}$ | 2D distance between the ABS and the user. |

performance of an IEEE 802.11a compatible OFDM for UAV downlink with large Doppler shift and inter-carrier interference (ICI) is analyzed. Similarly, the effect of ICI and inter-symbol interference from multi-path propagation are analyzed in [23] for OFDM based UAV data link communication in urban environment. The fast Fourier transform (FFT) size of OFDM is increased to improve system performance with synchronization requirements. Realistic end-to-end ray tracing simulations are shown considering an A2G channel. In [24], an OFDM waveform design using software defined radio is considered.

As previously mentioned, only [1] describes the impact of adopting GFDM in UAV downlink transmission. However, GFDM has been researched for other use-cases and communication systems. In [25], the authors implement spread spectrum GFDM for integrated satellite-terrestrial communication and conduct performance analysis with SER and peak-to-average-power-ratio. Similar analysis is done with the same performance indicators and spectral efficiency in [26] for underwater acoustic channels considering different pulse shaping filters. Further, DC biased Optical GFDM has been proposed for visible light communication in [27] with performance analysis under double sided clipping. For improving the energy efficiency of internet-of-things (IOT) devices, radio resource allocation with wireless information and power transfer scheme has been addressed for multiuser GFDM system model in [28].

Apart from academic research, industrial experiments were performed by various companies to provide cellular and internet connectivity through aerial platforms. Qualcomm was able to demonstrate smooth handovers with zero link failures with autonomous drone control over LTE network [29]. Facebook Aquila project conducted successful flights with solar powered drones to provide internet connectivity in suburban areas at an altitude of $18-20$ Km with pre-defined waypoints to provide a cell coverage area of nearly $100$ Km [30]. Aquila used free space optical links to ground access points which further connected to mobile users using Wi-Fi or LTE technology. Also, Nokia worked on the project of "Connected UAVs" to implement a swarm and collision avoidance technology, which has multiple use cases in smart cities, transportation, search and rescue, etc [31].

### C. Contributions

The main contributions of this paper are as follows:

- We compute an optimal altitude of the ABS for minimum SER and maximum ABS cell coverage in different environments. The optimal altitude is obtained from a static ABS by performing ray tracing simulations at different heights. However, the three dimensional propagation environment makes the channel results site-specific. We have eliminated this limitation by creating generalized environments, which are described in Sec. IV. Therefore, our results can be implemented for any realistic environments.
- We implement GFDM in our system model for ABS downlink performance analysis, as being considered the

most suitable and compatible waveform for LTE, LTE-A, and LTE-Pro hybrid systems [32] due to its backward compatibility with the forth generation (4G) frame structure. We use parameters of low latency communication (higher sub-carrier spacing and lower symbol duration) of physical layer (PHY) as given in Table III.
- We use A2G channel parameters for SER calculations in the GFDM model. We also provide the power delay profiles for A2G channel in different environments at the optimal altitude. For obtaining the A2G channel, similar ray tracing simulations were performed with static and moving ABS. Further, the distribution of the received power for ground receivers in different environments is also computed using the optimal ABS altitude, which supplements to find the variation of optimal altitude with cell radius.
- Finally, we implement various BTN pulse shaping filters in the GFDM transceiver to obtain SER at optimal ABS altitude and show significant performance gains as compared to Nyquist pulse shaping filters. These simulations were conducted for both static and moving ABS, to analyze the effect of Doppler shift on SER.

The rest of the article is organized as follows. In Sec. II, we address the GFDM system model for LAP A2G channel model. Section IV, describes the ray tracing simulation setup developed with various environmental and transceiver parameters. In Sec. V, we perform a trade-off analysis to obtain optimal ABS altitude for maximum cell coverage and minimum SER. We also provide the analytical expression of optimal altitude, the power delay profile, and the parameters of the received power distribution of ground users. Further, in Sec. VI we report various pulse shaping filters and present results to obtain the minimum SER in different environments. To the best of our knowledge, this article presents a unique study of performance analysis for ABS with different optimal altitude determination criterion, which has not been addressed in the existing literature. The symbols and the notation used in this paper are addressed in Table I for quick reference.

## II. System Model

In the context of vehicular communication systems, both LTE vehicle-to-everything (V2X) [33] and the Wi-Fi based IEEE 802.11p [34] solutions implement OFDM modulation, which is characterized by high out-of-band (OOB) emission. In case of transmission over highly time and frequency selective fading channels, the performance of OFDM is severely impaired by channel estimation and synchronization errors. Therefore, OFDM may not be a desirable waveform for UAV communications in terms of inefficient usage of time and frequency resources [35]. Thus far, it is well known that GFDM is one of the multi-carrier schemes under consideration for the future networks architectures. Due to its low OOB emission obtained by circular pulse shaping filter, GFDM improves the spectral efficiency in short data burst transmission with ultra low latency scenario [32]. A characteristic of GFDM is that of being backward compatible with OFDM and single-carrier frequency division multiple access (SC-FDMA).

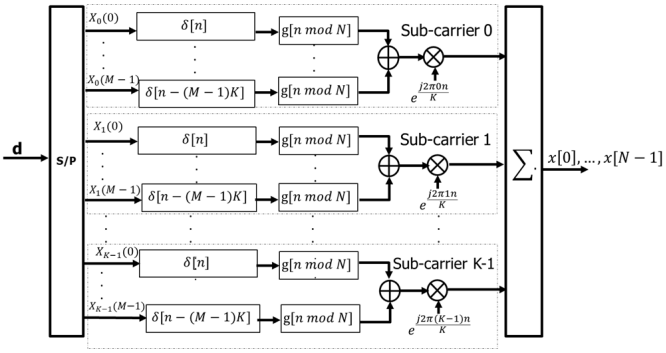


Fig. 2. GFDM modulator block diagram [36].

Hence, we implement GFDM in our simulations. In the GFDM transmission scheme [36], the high data-rate stream in vector $\mathbf{d}$ contains $N$ elements, which can be further decomposed into low symbol-rate streams of $K$ sub-carriers with $M$ sub-symbols each, by applying $\mathbf{d}$ to the GFDM modulator. As shown in Fig. 2, the input of the GFDM modulator is given by

$$\mathbf{d}=[\boldsymbol{d}_0,\, \mathbf{d}_1, \ldots ...,\mathbf{d}_{K-1}]^T,$$

where

$$\mathbf{d}_k=[d_{k,0},\, d_{k,1}, \ldots ..,d_{k,M-1}]^T,$$

with $(\cdot)^T$ being the transpose operator and $d_{k,m}$ the $m^{th}$ complex sub-symbol transmitted on $k^{th}$ sub-carrier of the block. The total number of symbols is $N = KM$. The sub-carrier spacing is equal to $1/T_s$ and time-period of each data block $\mathbf{d}_k$ is $MT_s$, where $T_s$ is sub-symbol duration.

The transmitted signal at the discrete-time index $n$ is given by

$$x\,[n] = \sum_{k=0}^{K-1} \sum_{m=0}^{M-1} d_{k,m} g_{k,m}\,[n], n= 0, 1, \ldots ..KM-1, \quad (1)$$

where $g_{k,m}[n]$ is the corresponding pulse shaping filter

$$g_{k,m}\,[n] = g\,[(n-mK) \bmod N]\, e^{\frac{-\mathrm{j}2\pi \mathrm{kn}}{K}},$$

with $g\,[n]$ representing the prototype filter and $\bmod$ denoting the modulo *N* operation, which makes $g_{k,m}\,[n]$ a circularly shifted version of $g_{k,0}\,[n]$. The exponential function performs the frequency shifting operation and *n* is the sampling index.

By collecting *N* samples of $g_{k,m}[n]$ in the matrix form, the vector representation of (1) can be written as

$$\mathbf{x} = \mathbf{A}\,\mathbf{d}, \quad (2)$$

where $\mathbf{x} = [x[0], x[1], \cdots, x[N-1]]^T$, and $\mathbf{A} = \left[\boldsymbol{g}_{0,0} \cdots \boldsymbol{g}_{K-1,0}\ \boldsymbol{g}_{0,1}\ \ \boldsymbol{g}_{K-1,1}\ \ \boldsymbol{g}_{0,M-1} \cdots \boldsymbol{g}_{K-1,M-1}\right]$.

Before transmitting over the A2G channel, the cyclic prefix (CP) of length $N_{CP}$ is added to create the vector given as

$$\widehat{\boldsymbol{x}} = \left[\mathbf{x}\,(N-N_{CP}:N-1)^T, \mathbf{x}^T\right]^T. \quad (3)$$

The CP length is taken equal as the number of taps in the channel for our simulations, *i.e*, 10 as reported in Table II.

Further, transmission with propagation effects such as path loss and large scale fading effects over A2G probabilistic channel [13] can be modeled as

$$\mathrm{PL_{LoS}}(\varphi)[\mathrm{dB}]=20\log_{10}\left(\frac{4\pi\varphi_0}{\lambda}\right)+10\eta_{\mathrm{LoS}}\log_{10}(\varphi)+X_{\sigma,\mathrm{LoS}}, \tag{4}$$

$$\mathrm{PL_{NLoS}}(\varphi)[\mathrm{dB}]=20\log_{10}\left(\frac{4\pi\varphi_0}{\lambda}\right)+10\eta_{\mathrm{NLoS}}\log_{10}(\varphi)+X_{\sigma,\mathrm{NLoS}}, \tag{5}$$

where LoS and NLoS denote line-of-sight and non-LoS, respectively, with $\eta$ being the path loss exponent (PLE), PL representing the path loss, $\varphi$ denoting the distance between ground receiver and ABS with $\varphi_0$ as the reference distance, assumed here as $\varphi_0 = 1$. $X_\sigma$ represents the log-normal shadowing where $\sigma$ is the standard deviation which includes the large scale fading effects. Thus far, the average PL model can be obtained as

$$\mathrm{PL}(\varphi)[\mathrm{dB}] = \mathbb{P}_{\mathrm{LoS}}\cdot\mathrm{PL_{LoS}}(\varphi) + (1-\mathbb{P}_{\mathrm{LoS}})\cdot\mathrm{PL_{NLoS}}(\varphi), \tag{6}$$

where $\mathbb{P}_{\mathrm{LoS}}$ is the LoS probability of the link [16] which is modeled as

$$\mathbb{P}_{\mathrm{LoS}} = \frac{1}{1+\omega\exp(-\varepsilon[\phi-\omega])}, \tag{7}$$

being $\omega$ and $\varepsilon$ the parameters of the LoS curve, depending on the environment structuring variables, $\alpha$, $\beta$ and $\gamma$ as given in Sec. IV and $\phi$ being the elevation angle between the ABS and the ground user, depending on the type of antenna used as shown in Fig. 1. The channel parameters such as PL and $X_\sigma$ in different environments and UAV altitudes were obtained from ray tracing simulations, as will be explained in Sec. IV. However, this model does not include the small scale fading effects.

The coefficients of the discrete-time channel impulse response $h[n]$ are usually modeled as Ricean for A2G channel [37]. In fact, $h[n]$ can be derived via stochastic methods through empirical data, simulations, and geometric analysis [37]. Here, we implement the map-based approach to obtain the data and model $h[n]$ as

$$h[n] = \sum_{\upsilon=0}^{\Pi-1} h_\upsilon \delta[n-\upsilon], \tag{8}$$

where $\delta[n]$ is the Kronecker delta and $h_\upsilon$ is the $\upsilon^{th}$ complex Ricean fading coefficient, which is evaluated via ray tracing channel propagation data as $\mathrm{PG} = -(\mathrm{PL_{tot}}(\varphi)[\mathrm{dB}] - (\mathbb{P}_{\mathrm{LoS}}\cdot\mathrm{PL_{LoS}}(\varphi) + (1-\mathbb{P}_{\mathrm{LoS}})\cdot\mathrm{PL_{NLoS}}(\varphi)))$ and $\Pi$ represents the number of channel taps. PG denotes the channel power gain for each channel tap and $\mathrm{PL_{tot}}(\varphi)[\mathrm{dB}]$ shows the total PL including both shadowing and multipath fading effects. At the GFDM receiver, we scrutinize the CP length should be greater than the maximum delay spread of the A2G channel, i.e, $N_{CP} \geq \Pi$. Under such presumption and after removing the CP, the received signal vector can be written as

$$\mathbf{y} = \mathbf{H}\mathbf{x}+\mathbf{w}, \tag{9}$$

where $\mathbf{H}$ denotes the circulant matrix of size $N\times N$ based on $\mathbf{h}$, which is $(N\times 1)$ vector where first $\Pi$ elements represent channel impulse response and the remaining $N-\Pi$ are null. Further, $\mathbf{w}$ represents the noise vector of size $N\times 1$ where every element is an independent and identically distributed Gaussian random variable with zero mean and variance $\sigma_w^2$. Under the consideration of Matched Filter (MF); the equalized signal in time domain using the modulator matrix $\mathbf{B}_{MF} = (\mathbf{A}^H\mathbf{A})^{-1}\mathbf{A}^H$, the estimated data vector is

$$\hat{\mathbf{d}} = \mathbf{B}_{MF}\mathbf{y}_{eq} = \mathbf{B}_{MF}\mathbf{A}\mathbf{d} + \mathbf{B}_{MF}\mathbf{H}^{-1}\mathrm{w} \tag{10}$$

where $\mathbf{y}_{eq}$ is the equalized signal in time-domain and MF receiver maximizes the Signal to Noise-Ratio (SNR) per subcarrier.

TABLE II
RECEIVED POWER DELAY PROFILE WITH DELAY IN "NS" AND POWER IN "DB" AT OPTIMAL ALTITUDE FOR 10 TAP CHANNEL

| Suburban scenario | | Urban scenario | | Urban High Rise scenario | |
|---|---|---|---|---|---|
| Delay | Power | Delay | Power | Delay | Power |
| 2100 | -66.44 | 1450 | -23.51 | 2023 | 151.09 |
| 2530 | -51.51 | 1496 | 14.35 | 2131 | 111.76 |
| 2595 | 25.67 | 1645 | 6.98 | 2324 | 80.49 |
| 2826 | -19.77 | 1703 | -56.25 | 2429 | 76.64 |
| 2836 | -57.51 | 1752 | -38.87 | 2732 | 92.23 |
| 3085 | -31.31 | 1784 | -71.12 | 2745 | 135.52 |
| 3390 | 22.59 | 1935 | -56.66 | 2916 | 115.11 |
| 3463 | 28.87 | 2055 | -41.83 | 3027 | 112.40 |
| 3870 | -48.47 | 2191 | -39.72 | 3105 | 82.96 |
| 3951 | -34.55 | 2346 | -63.87 | 3138 | 79.16 |

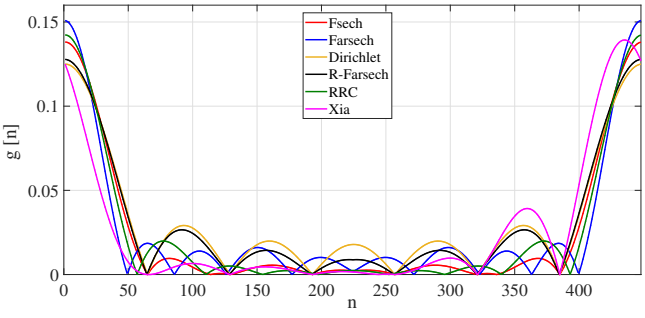


Fig. 3. Frequency response of the employed pulse shaping filters.

The spectral efficiency of the GFDM system is affected by the pulse shaping filter $g[n]$. Thus, we use BTN pulse shaping filters as reported in [38] and shown in Fig. 3. A standard approach for choosing the pulse shaping filter is to sample a continuous-time impulse response $g(t)$ windowed as

$$g_w(t) = \begin{cases} g_{wdown}(t), & 1 \leq t \leq KT_s, \\ g_{wup}(t), & (MK-K)Ts \leq t \leq (MK)T_s, \\ 0, & \text{otherwise}, \end{cases} \tag{11}$$

where $g_{wup}(t)$=$g_{pulse}(t)$, $g_{wdown}(t)$=1-$g_{pulse}(t)$ and $T_s$ symbol interval, being $g_{pulse}(t)$ one of the different types of pulse shaping filters reported below.

To evaluate the performance of our system, we will address a trade-off analysis in Sec. V to obtain the optimal altitude of the UAV. This will be based on the maximum cellular coverage with A2G probabilistic channel parameters obtained via ray tracing simulations in Sec. IV and minimum SER with

GFDM transmission scheme. Moreover, to address the impact on the SER performance of different BTN pulse shaping filters, in Sec. III we will show their time-domain expressions and in Sec. VI we will evaluate the performance by means of computer simulations.

## III. Pulse Shaping Filter

In this section, the pulse shaping filters used for performance assessment of the GFDM system model are addressed. Their time-domain expressions are given in the sub-sections that follows.

### A. Root raised cosine (RRC)

For the given roll-off factor $\Delta$, the time domain equation of the root raised cosine (RRC) filter is given as

$$g_{RRC}(t) = \sqrt{g_{RC}(t)}. \tag{12}$$

where

$$g_{RC}(t) = \begin{cases} 1, & |t| \leq \frac{(1-\Delta)T_s}{2}, \\ \frac{1}{2}\left[1+\cos\left(\pi Q_{RC}(t)\right)\right], & \frac{(1-\Delta)T_s}{2} < |t| \leq \frac{(1+\Delta)T_s}{2}, \\ 0, & \text{otherwise}, \end{cases} \tag{13}$$

where $Q_{RC}(t)$ is the inner argument of cos, as given in [39].

### B. Flipped-hyperbolic secant (Fsech)

As proposed in [38], we implement the BTN pulse shaping filter, $Fsech$, which is defined as

$$g(t) = \begin{cases} 1, & |t| \leq \frac{(1-\Delta)T_s}{2}, \\ 1 - sech\left(\rho P_{1Fsech}(t)\right), & \frac{(1-\Delta)T_s}{2} < |t| \leq \frac{T_s}{2}, \\ sech\left(\rho P_{2Fsech}(t)\right), & \frac{T_s}{2} < |t| \leq \frac{(1+\Delta)T_s}{2}, \\ 0, & \frac{(1+\Delta)T_s}{2} < |t|, \end{cases} \tag{14}$$

where $sech$ being the hyperbolic secant function, $\rho = ln\left(\sqrt{3}+2\right)/\Delta \times \frac{T_s}{2}$ , $P_{1Fsech}(t)$ and $P_{2Fsech}(t)$ are the inner arguments of $sech$ as provided in [39].

### C. Flipped-inverse hyperbolic secant (Farcsech)

Furthermore, as proposed in [38], another implemented BTN pulse shaping filter is $Farcsech$, which is defined as

$$g(t) = \begin{cases} 1, & |t| \leq \frac{(1-\Delta)T_s}{2}, \\ arcsech\left(\frac{1}{\rho}\ P_{1Farcsech}(t)\right), & \frac{(1-\Delta)T_s}{2} < |t| \leq \frac{T_s}{2}, \\ 1 - arcsech\left(\frac{1}{\rho}\ P_{2Fsech}(t)\right), & \frac{T_s}{2} < |t| \leq \frac{(1+\Delta)T_s}{2} \\ 0, & \frac{(1+\Delta)T_s}{2} < |t|, \end{cases} \tag{15}$$

where $arcsech$ represents the inverse $sech$ function, $P_{1Farcsech}(t)$ and $P_{2Fsech}(t)$ are the inner arguments of $arcsech$ as provided in [39].

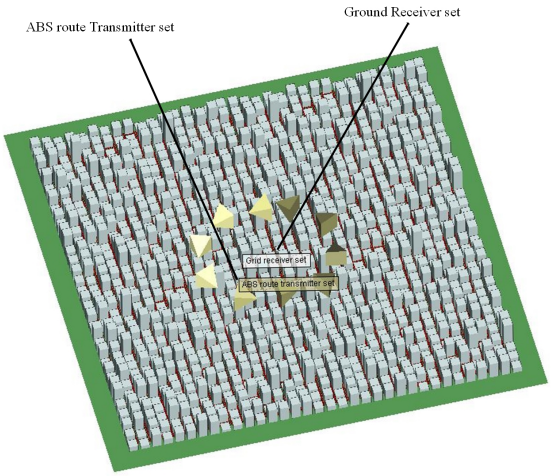


Fig. 4. Urban High Rise Scenario with moving ABS altitude of 600 m in Wireless InSite.

## IV. Ray Tracing Simulation Setup

The customized simulation setup was created to obtain the attributes of LAPs' A2G channel model with different ABS transmitting powers and altitudes. We develop three environments, i.e. Urban High Rise, Urban, and Suburban, on 3DS MAX, a Computer-Aided-Design (CAD) software, according to the parameters provided by ITU-R [40]:

- $\alpha$ = Proportion of field area covered by the infrastructure to the total area (dimensionless).
- $\beta$ = Average number of buildings per unit area (building/ sq km).
- $\gamma$ = Variable to address the height distribution of the buildings. A Rayleigh distribution is proposed by ITU-R.

The values of $\alpha$, $\beta$ and $\gamma$ along with other city layout parameters, such as number of buildings, street width, building size, and material, are given in [13]. The CAD environments were of area $2000 \times 2000\ \text{m}^2$, from which ray tracing was done over $1000 \times 1000\ \text{m}^2$ at various points. Two set of simulations were performed - moving and static ABSs. For static ABS, it was presented at the center of the snapshot, with approximately $33,000$ receivers spread uniformly over the entire surface of the environment with 5 m spacing from each other. There were no receivers inside buildings, since outdoor propagation was studied to support flash crowds. For moving ABS, a circular trajectory of ABS was considered, as shown in Fig. 4. The buildings' height and density were most in Urban High Rise environment and least in the Suburban. Also, conventional earth materials and concrete were implemented for terrain and buildings, respectively. The ray tracing simulation was conducted in Wireless InSite 3.0.1 [41], a commercial software radio wave propagation. The accuracy of practical measurements from the software is well defined in [42]. The simulations were performed in the 2.4 GHz unlicensed band with 20 MHz bandwidth for UAV heights up to 2000 m altitude, with step of 100 m, and transmission power in the range from 18 to 46 dBm, at every 2 dBm interval. The simulations were conducted in sub-6 GHz as it was preferred in 3GPP [7],

TABLE III
PARAMETERS FOR GFDM SIMULATION WITH LTE GRID [32]

| Parameter | Normal mode |
|---|---|
| Subframe duration | 1 ms or 30.720 samples |
| GFDM symbol duration | 66.67 $\mu$s or 2048 samples |
| Subsymbol duration | 4.17 $\mu$s or 128 samples |
| Subcarrier spacing | 240 KHz |
| Subcarrier bandwidth | 240 KHz |
| Sampling freq. (clock) | 30.72 MHz |
| Subcarrier spacing factor $N$ | 128 |
| Subsymbol spacing $K$ | 128 |
| active subcarriers $N_{on}$ | 75 |
| Subsymbols per GFDM symbol $M$ | 15 |
| GFDM symbols per subframe | 15 |
| CP length | 4.17 $\mu$s or 128 samples |

where many field trials were conducted by industries. The unlicensed spectrum of LTE was adopted due to unavailability of dedicated spectrum for such ABS architecture. The average of results from various snapshots at each UAV height were taken to improve the accuracy of the results. The receivers outside the buildings were only considered for the simulation. Figure 4 shows a snapshot of the simulation in Urban High Rise environment. Further, Table II, refers to the received power delay profile of ground user at optimal altitude of the ABS. The antenna on the UAV was taken to be isotropic with 2 dB gain to remove directivity effects on the A2G channel measurements.

## V. TRADE-OFF ANALYSIS FOR OPTIMAL ALTITUDE OF ABS

In this section, we obtain the optimum altitude of an ABS by focusing on two different parameters - minimum SER and maximum ABS cell coverage area. For obtaining the SER, we use a flexible multi-carrier modulation scheme, GFDM, where the sub-carriers are individually pulse-shaped in a block structure of K sub-carriers and M sub-symbols.

### *A. Optimal Altitude for Maximum Cell Coverage by ABS*

Here, we derive a closed-form expression for the optimal altitude of the ABS. The variation of the cell coverage with height of ABS is given in Fig. 5(a), where $300 - 400\,\mathrm{m}$ was observed as an optimal altitude for the same ray tracing simulations, in different environments. Reference [43] considers a generic received power threshold approach, where the cell coverage depends on the distance between the ABS and ground users receiving power, greater than the threshold required to maintain connectivity with the ABS. However, such an approach is implementable for any power source to define its boundaries. Therefore, we report a novel equation using a solid angle approach, taking into account A2G channel, antenna characteristics, ABS altitude, transmission power, and elevation angle with respect to users.

**Lemma 1:** The expression of cell area covered by an ABS is given by

$$A = \frac{2h^2}{R}\left(\sec\left(\phi_{max}\right) - 1\right) \left[\left(\frac{1-\mathrm{erf}(a)}{2}\right) - \frac{1}{2}\exp\left(\frac{1-4ab}{4b^2}\right)\left[\mathrm{erf}\left(\frac{1}{2b} - a\right) - 1\right]\right], \tag{16}$$

where $h$ is the height of ABS, $R$ is the radius of an area used for normalizing ABS cell area, erf is the error function, $a$ and $b$ are substitution parameters, given as

$$a = \frac{1}{\sigma\sqrt{2}}(P_{th}[dB] - P_{TX}[dB] - G_T[dB] - G_R[dB] + \mathrm{PL}_0[dB] + 10\eta\log_{10}(R/r_0)), \tag{17}$$

$$b = \frac{10\eta\log_{10}(e)}{\sigma\sqrt{2}}, \tag{18}$$

with $P_{th}$ is the received power threshold of ground users to maintain ABS link connectivity, $P_{TX}$ is the transmitted power by ABS, $G_T$ and $G_R$ are the transmitting and receiving antenna gains, respectively, PL is further written as a function of reference path loss $\mathrm{PL}_0$, at distance $r_0$ from the transmitter, as per close-in reference distance path loss model [44].

**Proof:** In order to obtain (16) we utilize a solid angle approach, where solid angle ($\Omega$) [45] is a 3D analogue of an angle, enclosed by a conical surface at the apex as shown in Fig. 1. The solid angle subtended by an element on the ground at ABS is given by

$$d\Omega = \frac{d\vec{A}}{\mathbf{d}^2}\cdot\hat{n}, \tag{19}$$

where $\mathbf{d}$ is the 3D distance or the slant height of the cone formed from the geometry and $\hat{n}$ is the unit vector from the origin. From (19) we have $dA = \sin\phi\,\mathbf{d}^2\,d\theta\,d\phi$, where $d\theta$ and $d\phi$ are azimuth and elevation angles, respectively. This relationship is only based on geometrical aspects. Therefore, the probability parameter $\mathbb{P}(P_{RX}(\mathbf{r}) \geq P_{th})$ is added to the above expression. This produces the actual coverage by the ABS. This parameter denotes the probability that the received power by the ground user $P_{RX}(\mathbf{r})$ is greater than $P_{th}$ and $\mathbf{r}$ is the 2D distance between the ABS and the user. Thus, we have

$$dA = \sin\phi\,\mathbf{d}^2\,\mathbb{P}(P_{RX}(\mathbf{r}) \geq P_{th})\,d\theta\,d\phi\,dr. \tag{20}$$

Thereby, integrating (20) under respective integral limits for minimum and maximum of each variable and normalizing the cell coverage, we have

$$A = \frac{\mathbf{d}^2}{A_C}\int_{\phi=0}^{\phi=\phi_{max}}\sin\,\phi\,d\phi\int_{\theta=0}^{\theta=2\pi}d\theta\int_0^R\mathbb{P}(P_{RX}(\mathbf{r}) \geq P_{th})dr, \tag{21}$$

where $R$ corresponds to $\phi_{max}$. $A_C = \pi R^2$ is the cell area used to normalize the final cell coverage $A$. Thus, from (21) we have

$$A = \frac{2\pi h^2}{A_C}\int_{\phi=0}^{\phi=\phi_{max}}\frac{\sin\,\phi}{\cos^2\phi}\,d\phi\int_0^R\mathbb{P}(P_{RX}(\mathbf{r}) \geq P_{th})dr.$$

TABLE IV
PROBABILITY DISTRIBUTION PARAMETERS OF RECEIVED POWER AT OPTIMAL ALTITUDE

| Environment | Optimal Altitude [m] | Distribution type | Distribution parameters | | | |
|---|---|---|---|---|---|---|
| | | | $\mu$ (location) | $\sigma$ (scale) | $\nu$ (degrees of freedom) | $k$ (shape) |
| Suburban | 600 | t location-scale | $-94.9520$ | 2.5348 | 1.7666 | - |
| Urban | 400 | Extreme Value | $-75.7450$ | 6.0756 | - | - |
| Urban High Rise | 600 | Generalized Extreme Value | $-95.5724$ | 15.5478 | - | $-0.5446$ |

Now integration of each part is shown separately as

$$A = \frac{2\pi h^2}{A_C} I_1 I_2 \tag{22}$$

where

$$I_1 = \int_{\phi=0}^{\phi=\phi_{max}} \frac{\sin\phi}{\cos^2\phi}\, d\phi = \sec(\phi_{max}) - 1 \tag{23}$$

and

$$I_2 = \int_0^R \mathbb{P}(P_{RX}(\mathbf{r}) \geq P_{th}) dr. \tag{24}$$

The term $I_2$ can be calculated using Q-function as $\mathbb{P}(P_{RX}(\mathbf{r}) \geq P_{th}) = Q\left(\frac{P_{th} - \overline{P}_{RX}(\mathbf{r})}{\sigma}\right)$. The Q-function is defined in the form of error function as

$$Q(x) = \int_x^\infty \frac{1}{\sqrt{2\pi}} \exp\left(-\frac{y^2}{2}\right) dy = \frac{1}{2}\left[1 - \text{erf}\left(\frac{x}{\sqrt{2}}\right)\right].$$

By replacing $x$ with $\left(\frac{P_{th} - \overline{P}_{RX}(\mathbf{r})}{\sigma}\right)$,

$$Q\left(\frac{P_{th} - \overline{P}_{RX}(\mathbf{r})}{\sigma}\right) = \frac{1}{2}\left[1 - \text{erf}\left(\frac{P_{th} - \overline{P}_{RX}(\mathbf{r})}{\sqrt{2}\sigma}\right)\right].$$

By further substitution with log-distance path loss model (in dB), $\overline{P}_{RX}(r) = P_{TX} + G_T + G_R - PL$, and by substituting for $PL$, we have,

$$\overline{P}_{RX}(r) = P_{TX} + G_T + G_R - \left(PL_0 + 10\eta \log_{10}\left(\frac{r}{r_0}\right)\right),$$

where $P_{TX}$ is the transmitted power, $G_T$ and $G_R$ are the transmitting and receiving antenna gain, respectively, PL is the path loss which is further written as a function of reference path loss $PL_0$, at distance $r_0$ from the transmitter, and path loss exponent $\eta$. Therefore, we have

$$\mathbb{P}(P_{RX}(r) \geq P_{th}) = \frac{1}{2}\left[1 - \text{erf}\left(\frac{P_{th} - \left[P_{TX} + G_T + G_R - \left[PL_0 + 10\eta\log_{10}\left(\frac{r}{r_0}\right)\right]\right]}{\sigma\sqrt{2}}\right)\right],$$

where we substitute the following for clarity

$$a = \left(\frac{P_{th} - P_{TX} - G_T - G_R + PL_0 + 10\eta\log_{10}(R/r_0)}{\sigma\sqrt{2}}\right)$$

$$\text{and} \quad b = \frac{10\eta\log_{10}(e)}{\sigma\sqrt{2}}.$$

Therefore, we represent

$$\mathbb{P}(P_{RX}(r) \geq P_{th}) = \frac{1}{2} - \frac{1}{2}\,\text{erf}\left(a + b\ln\frac{r}{R}\right) \text{ and}$$

$$I_2 = \int_0^R \mathbb{P}(P_{RX}(r) \geq P_{th}) dr = \int_0^R \frac{1}{2} - \frac{1}{2}\,\text{erf}\left(a + b\ln\frac{r}{R}\right) dr. \tag{25}$$

Replacing $t = a + b\ln\frac{r}{R}$

$$I_2 = \frac{R}{2} - \frac{R}{2b}\int_{-\infty}^a \exp\left(\frac{t-a}{b}\right)\text{erf}(t) dt.$$

Integrating by parts, we obtain

$$I_2 = R\left[\left(\frac{1 - \text{erf}(a)}{2}\right) - \frac{1}{2}\exp\left(\frac{1-4ab}{4b^2}\right)\left[\text{erf}\left(\frac{1}{2b} - a\right) - 1\right]\right].$$

Now substituting for $I_1$,$I_2$ and $A_C$ in (22), we finally get (16). From (22), the optimal height of ABS for maximum coverage can be obtained as $\frac{dA}{dh} = 0$. Therefore,

$$h = \frac{R^2}{4\, I_1\, I_2} \tag{26}$$

$$h = \frac{R}{4\,(\sec(\phi_{max}) - 1)\left[\left(\frac{1-\text{erf}(a)}{2}\right) - \frac{1}{2}\exp\left(\frac{1-4ab}{4b^2}\right)\left[\text{erf}\left(\frac{1}{2b} - a\right) - 1\right]\right]} \tag{27}$$

By implementing the parameters of simulations as given in [43], the curves of cell coverage with respect to ABS altitude from (16) were found to be similar. Therefore, we acknowledge $300 - 400$ m as the optimal altitude of ABS in different environments as shown in Fig 5 (a).

**Remark 1:** From (26), $I_1$ and $I_2$ cannot be equal to zero, for the equation to hold. Therefore, analytically from (23), $\sec\phi_{max} - 1 \neq 0 \Rightarrow \phi_{max} \neq \frac{n\pi}{2}$, where $n \subset \mathbb{Z}$ (set of integer values) and since $\phi$ is the elevation angle, max($\phi$) = $\frac{\pi}{2}$. Also from (24),

$\mathbb{P}(P_{RX}(\mathbf{r}) \geq P_{th}) = Q\left(\frac{P_{th} - \overline{P}_{RX}(\mathbf{r})}{\sigma}\right) \neq 0.$

$\Rightarrow \left(\frac{P_{th} - \overline{P}_{RX}(\mathbf{r})}{\sigma}\right) \leq 3$ or $P_{th} \leq 3\sigma + P_{RX}$, since $\lim_{x \geq 3} Q(x) \to 0$. Therefore, the threshold received power should not be greater than received power by three times the standard deviation of log-normal shadowing for (26) to be valid.

**Remark 2:** For mobile operators to use ABS network, they have to tune the parameters such as $P_{th}$, $P_{TX}$, $G_T$ and $G_R$ depending on the SER, height and ABS cell coverage required. From Fig. 5 (a) and (b), we can infer that at the desired value of SER, SER$_{th}$, a corresponding ABS altitude $h_{th}$ can be obtained, depending on the type of environment and waveform

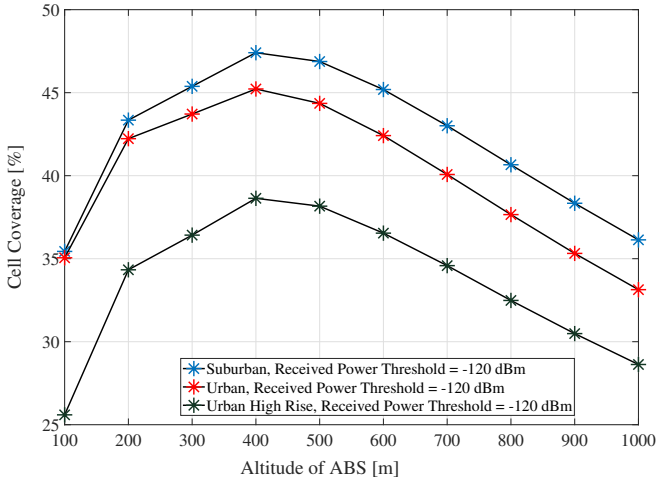


(a) Cell coverage variation with altitude of ABS.

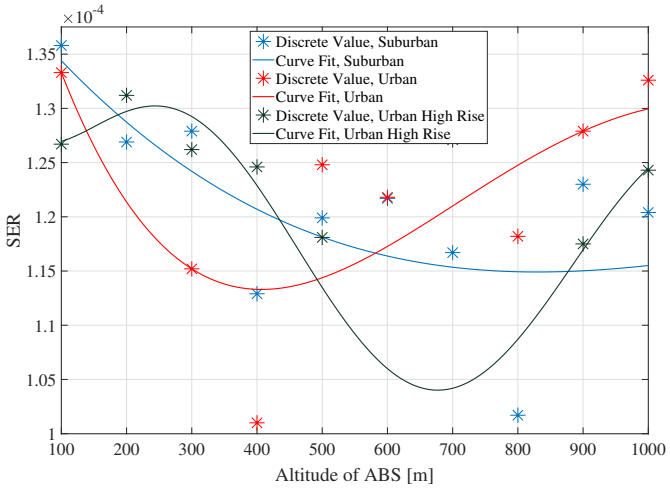


(b) SER variation with altitude of ABS.

Fig. 5. Trade-off between maximum cell coverage and minimum SER to obtain optimal altitude.

used for transceiver. Therefore, a geometrical coverage area $A'$ can be obtained excluding channel propagation effects as

$$A' = \pi R'^2 = \pi \left(h_{th} \tan\left(\phi_{max}\right)\right)^2$$

where $R'$ is the radius of ABS cell coverage. From (16), $A$ can be replaced by $A'$, and reorganized as follows

$$\frac{A'R}{2h^2\left(\sec\left(\phi_{max}\right)-1\right)} = \left[\left(\frac{1-\mathrm{erf}(a)}{2}\right) - \frac{1}{2}\exp\left(\frac{1-4ab}{4b^2}\right)\left[\mathrm{erf}\left(\frac{1}{2b}-a\right)-1\right]\right] \tag{28}$$

It is important to mention from (17) and (18), if $c = \frac{1}{\sqrt{2}}\left(10\eta\log_{10}(e) - 10\eta\log_{10}\left(\frac{R}{r_0}\right)\right)$ from **Lemma 1**, it will imply that $a = b$, where $c = \frac{P_{th}-P_{TX}-G_T-G_R+\mathrm{PL}_0}{\sqrt{2}}$. Also, for special case $R = e \times r_0$, $b$ from (18) can be rewritten in the form of $a$ defined in (17) as

$$b = a - \frac{c}{\sigma}. \tag{29}$$

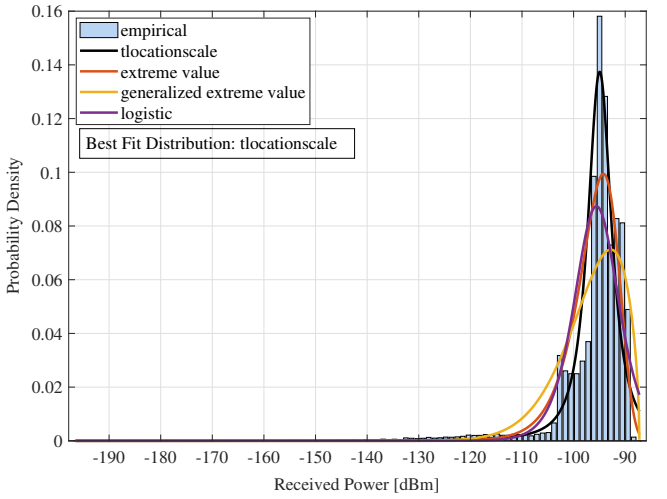


(a) Suburban Environment at ABS altitude of 600 m

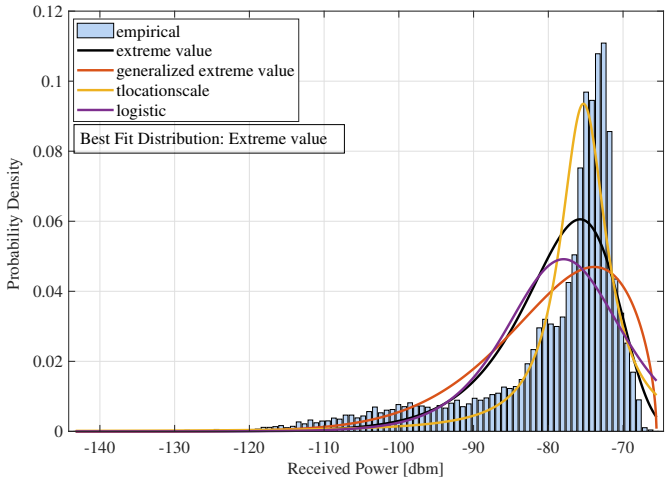


(b) Urban Environment at ABS altitude of 400 m

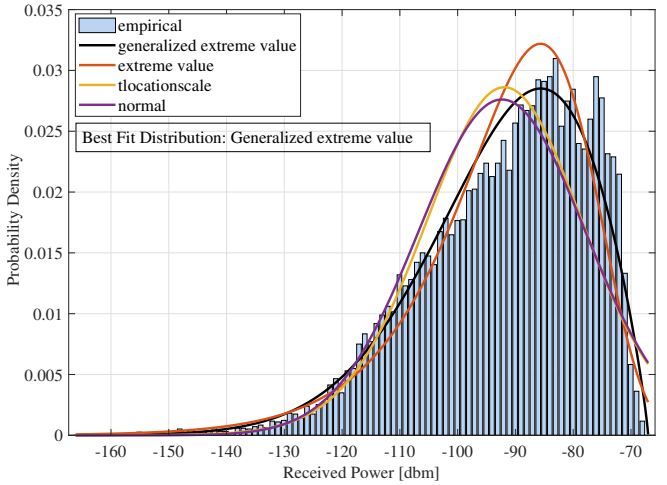


(c) Urban High Rise Environment at ABS altitude of 600 m

Fig. 6. Received power distribution of ground receivers in different environments at optimal ABS altitude.

Therefore, (28) can be rewritten as

$$F(a) - Y = 0, \tag{30}$$

where F(a) can be obtained by substituting $b$ from (29) into Right Hand Side (RHS) of (28) and $Y = \frac{A'R}{2h^2(\sec\phi_{max}-1)}$. We can easily find the root of (30), which will give us the value of $a$. The channel parameters such as $\eta$ and $\sigma$ can be obtained at different altitudes from [13].

### *B. Optimal Altitude for minimum SER by ABS*

In order to obtain the optimal altitude for the minimum SER, a GFDM transceiver system on an LTE grid was implemented by considering a low latency scenario. The parameters of the simulation have been taken from [32], and are provided in Table III. Reference [32] also describes the implementation of GFDM for a low latency scenario, where the main approach is to reduce the GFDM symbol duration and add a single cyclic prefix for the $M$ sub-symbols. Here, the GFDM symbol duration was kept to $1$ ms subframe duration. Based on these parameters, SER simulations were carried out for Suburban, Urban, and Urban High Rise environments to obtain optimal ABS altitude, with different power delay profiles at different altitudes. These profiles were obtained from ray tracing simulations for probabilistic A2G LoS channel model. We consider a Ricean fading model since LoS probability increases with increase in ABS altitude [16]. In Fig. 5(b), we plot the SER versus the ABS altitude for the considered environments as discrete values and obtain a curve fit to show the variation. We observe less variation of SER with altitude for Suburban scenario as compared to Urban and Urban High rise scenarios, which is probably due to the higher LoS probability in Suburban than Urban and Urban High Rise [16]. This implies that the ground users would receive an LoS ray component of the Ricean channel with higher probability, which also increases with the ABS altitude, thereby producing lower variation in SER with ABS height. Conversely, in Urban and Urban High Rise scenarios, the SER variation is high due to low LoS probability, which tend to increase the effect of scattered components of multipath. Also the range in y-axis is limited in Fig. 5(b) due to the frequency-flat fading scenario observed for ABS. As can be seen from Fig. 5(b), the optimal altitude for minimum SER is as follows: Suburban - $800$ m, Urban - $400$ m and Urban high Rise - $800$ m.

### *C. Optimal Altitude with varying Cell Radius for different Received Power Thresholds*

As observed in Secs. V-A and V-B, the optimal altitude of ABS has to be a trade-off for maximum coverage and minimum SER which we report in Table IV. In this section we address the probability distributions of the received power of ground users at optimal altitude of ABS, which are given in Fig. 6. The received power has been obtained from ray tracing simulations as described in Sec. IV. The received power was fitted with several probability distributions such as Normal, Nakagami, Rayleigh, Ricean, Exponential, Beta, Birnbaum-Saunders, Extreme value, Generalized extreme value, Gamma, t location-scale, Weibull, Logistic, Gaussian etc. From all these distributions the closest and best fit distribution is shown in Fig. 6. The parameters of the distributions are provided in Table IV. With such parameters, the received power can be extracted as random values without performing ray tracing simulations or practical measurements. These values were used to obtain the variation of optimal ABS altitude $h$ with respect to cell radius $R$ for all considered environments as shown in Fig. 7. The behavior of the curves expects to follow (27), where $h$ depends on $R$ and substitution parameter $a$, which also depends on $R$. However, [16] shows a linear variation of the optimal LAP altitude with the radius of the cell when constrained on maximum allowed path loss, which is the threshold value for maintaining the link connectivity. This is different from our approach since we consider minimum SER and maximum cell coverage constraints for obtaining optimal altitude. Here, we also show the variation with received power threshold of ground users. We observe, for higher thresholds, a high optimal altitude is required to cover the same cell radius with minimum SER. Also, the optimal altitudes for Suburban and Urban High Rise are higher than Urban, as shown in Fig. 7 and Table IV.

In this section, the considered trade-off is between ABS cellular coverage and SER in GFDM transmission, as the fundamental key performance indicators of our system model. However, to improve it further, more complex optimization problems can be developed by including other parameters, which are described as a part of our future work in Sec. VII.

## VI. Performance evaluation with "Better than Nyquist" Pulse shaping filters

The choice of pulse shaping filters strongly affect the spectral properties of a signal. The most commonly used Nyquist pulse is raised cosine pulse. Here, we have implemented BTN pulses such as Flipped-hyperbolic secant (Fsech), Flipped-inverse hyperbolic secant (Farcsech) and Reverse-Farcsech (R-Farcsech) pulse shaping filters which enables GFDM to achieve better SER performance as compared to raised-cosine pulse [39]. These filters were proposed in [46] to improve sensitivity to timing jitter in the context of single-carrier modulation. We compare results of these filters with Root-raised cosine and Xia pulses.

Figure 8 shows the SER analysis using the BTN filters for the three considered environments at optimal altitude of static ABS. We use the power delay profile given in Table II and Ricean factors given in [13], as A2G channel parameters for this simulation. We observe that ABS downlink at 2.4 GHz frequency band, follows a frequency-flat fading channel. Also, SER was found to be lower for all SNR values, for ABS downlink communication as compared to terrestrial one [38]. From Fig. 8, we also observe that SER is higher for Suburban environment, lower for Urban and least for Urban High Rise environment, for optimal altitude. This can also be addressed from Fig. 5(b). This is probably due to higher optimal altitude in Suburban scenario than Urban environments, chosen according to two different criterion as mentioned in previous sections. Therefore, this addresses for an effective use of ABS in Urban environments. We also address the results with moving ABS with maximum Doppler shift of 3,704 Hz, as shown in Fig. 10, which implies the ABS is cruising with very high speed relative to the ground

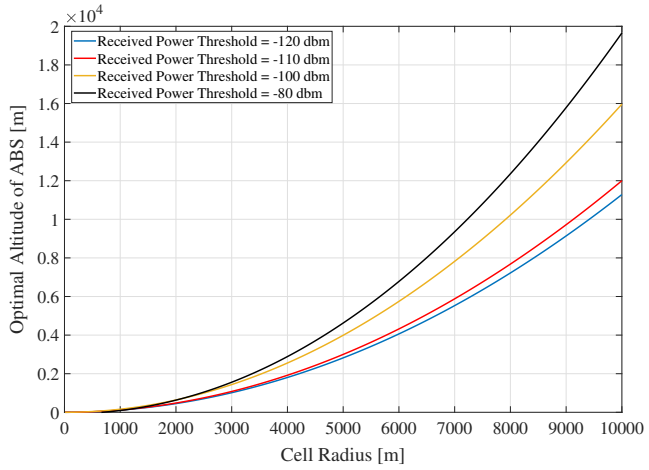


(a) Suburban environment.

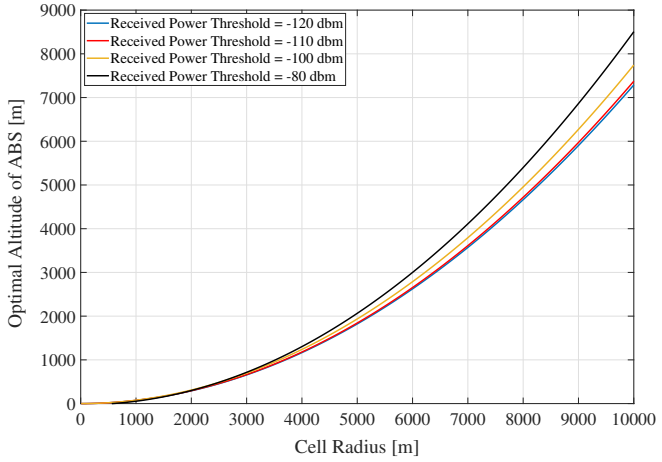


(b) Urban environment.

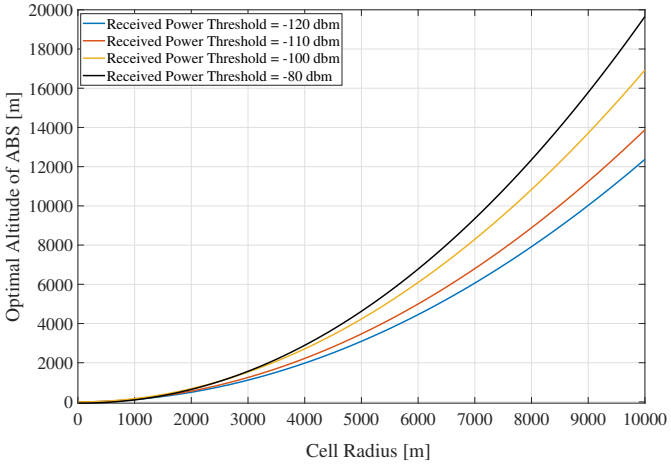


(c) Urban High Rise environment.

Fig. 7. Optimal ABS altitude variation with cell radius.

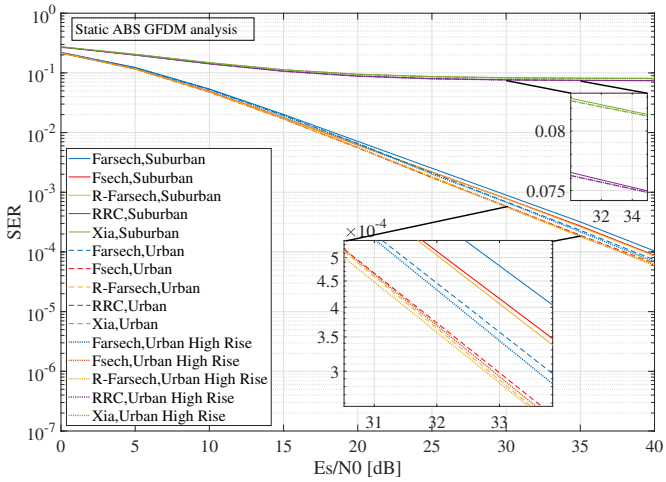


Fig. 8. GFDM SER analysis for static ABS.

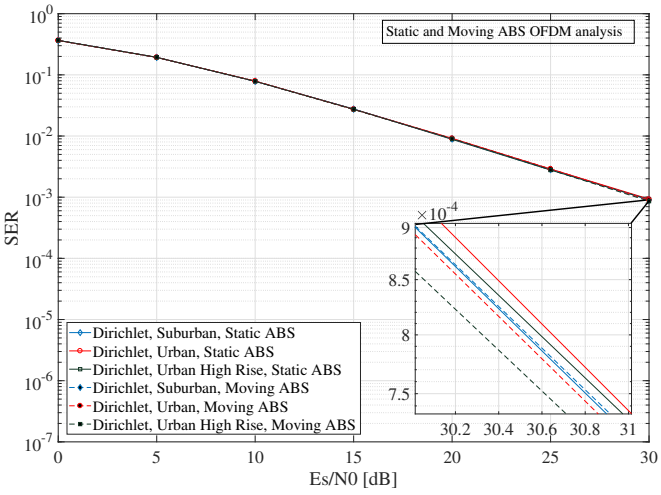


Fig. 9. OFDM SER analysis for static and moving ABS.

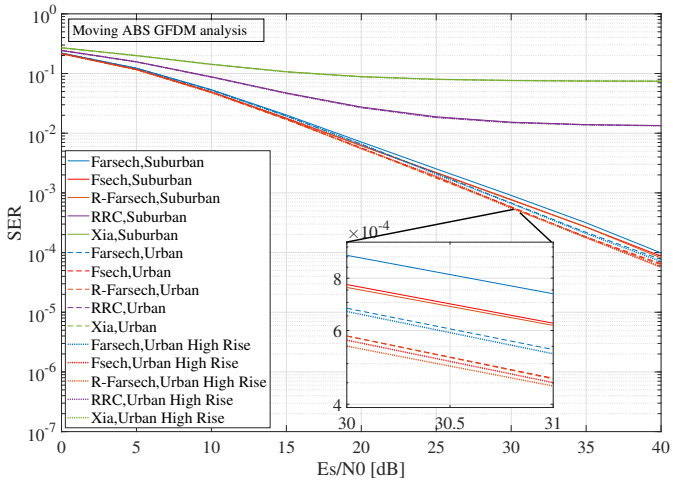


Fig. 10. GFDM SER analysis for moving ABS.

users. With such fast mobility, the coherence time of the multipath channel is expected to decrease and Doppler shift to increase. However, we did not observe large variations in moving ABS as compared to static ABS due to frequency-flat fading scenario, although SER values were found to be higher. Further, we implement a circular trajectory of the ABS to achieve uniformity in its motion, to eradicate any possible inaccuracy in the received power of the ground users

in ray tracing simulations due to sharp trajectory deviations. Also, homogeneity of ITU-R specified environments ensure the certainty of the results. Therefore, even with complex trajectories, similar channel measurements and SER results are expected.

It is possible to obtain the OFDM waveform from the GFDM one, by setting the number of sub-carriers to $K = 64$ and the number of sub-symbols to $M = 1$ with Dirichlet pulse shaping filter. We have performed simulations with static and moving ABS with the same maximum Doppler shift considered in GFDM system, as shown in Fig. 9. The simulation parameters were taken from [22], considering the maximum relative movement between the ABS and user. We observe that a similar behavior was obtained as reported in [22] with certain deviation since we use realistic A2G channel parameters obtained from ray tracing. This also provides insight to the validation of our OFDM and GFDM simulations. It is also significant to scrutinize that Wi-Fi also operates at $2.4\,$GHz carrier frequency. However, Wi-Fi based PHY is challenging to provide reliability in vehicular communication [35]. Also, as shown in [35], GFDM performs better than OFDM with Wi-Fi parameters due to higher throughput and better spectral and temporal characteristics. This implies GFDM has a better performance than OFDM at $2.4$ GHz band.

To summarize, we enhance the performance of ABS downlink communication system by addressing its optimal altitude for maximum coverage and minimum SER with implementation of GFDM waveform and BTN pulse shaping filters. Our solution can be implemented in real-time, where mobile operators can deploy ABS network, either as independent ABSs or to support the terrestrial network, with defined altitudes, waveforms, and suitable pulse-shaping to optimize the performance based on different data requirements of ground users. The main advantage is the possibility of relaying on closed-form expressions of ABS cellular coverage, BTN pulse-shaping filters, GFDM transmission scheme with simulation and channel parameters.

## VII. Conclusion and Future Work

In this article, we have shown the Symbol Error Rate (SER) analysis of LTE-Compatible GFDM, under low-latency scenario with GFDM symbol duration of 66.67 $\mu s$ and "Better than Nyquist" pulse shaping filters for a static and moving Aerial Base Station (ABS) providing cellular connectivity to ground users. We also address the SER results for OFDM. We have performed these simulations in different generalized environments- Suburban, Urban, and Urban High Rise, developed according to ITU-R parameters, at optimal altitude of ABS. The optimal altitude was defined based on two criterion's'- maximum cell coverage and minimum SER. Also, Air-to-Ground channel parameters were used to obtain SER simulation results, obtained from ray tracing results on a commercial radio propagation software. The power delay profile and probability distribution parameters of received power were also provided at the optimal altitude to reproduce the entire set of results without redoing the whole stack of operations. This also supplemented to show the variation of optimal altitude with cell area. For future works, we resort to hardware implementation for quantitative analysis to generate proof of concepts for algorithms implemented in this article. We also realise the importance to include other possible tradeoffs and their dependency on metrics such as energy efficiency, millimeter wave transmission, and directional antenna models to define a more complex optimization problem to find the ABS optimal altitude. Further, we plan to evaluate the features of other waveforms such as Universal Filtered Multi-Carrier (UFMC) and Filter Bank Multi-carrier (FBMC) modulations for various UAV use-case scenarios in heterogeneous network.

## Acknowledgment

This project has received funding from the NATO-SPS funding grant agreement No. G5482 and the European Union's Horizon 2020 research and innovation program under grant agreement No. 951867 and is also partly supported by European Union Regional Development Fund in the framework of the Tallinn University of Technology Development Program 2016–2022, code2014-2020.4.01.16-0032. This material reflects only the authors view and the EC Research Executive Agency is not responsible for any use that may be made of the information it contains.

## References

[1] N. Sharma, A. Kumar, M. Magarini, S. Bregni, and D. N. K. Jayakody, "Impact of CFO on Low Latency-Enabled UAV Using "Better Than Nyquist" Pulse Shaping in GFDM," in *IEEE 89th Vehicular Technology Conference (VTC2019-Spring)*, April 2019, pp. 1–6.

[2] S. Chandrasekharan, K. Gomez, A. Al-Hourani, S. Kandeepan, T. Rasheed, L. Goratti, L. Reynaud, D. Grace, I. Bucaille, T. Wirth, and S. Allsopp, "Designing and implementing future aerial communication networks," *in IEEE Communications Magazine*, vol. 54, no. 5, pp. 26–34, May 2016.

[3] S. Hayat, E. Yanmaz, and R. Muzaffar, "Survey on Unmanned Aerial Vehicle Networks for Civil Applications: A Communications Viewpoint," *in IEEE Communications Surveys Tutorials*, vol. 18, no. 4, pp. 2624–2661, Fourthquarter 2016.

[4] R. Gupta, A. Kumari, S. Tanwar, and N. Kumar, "Blockchain-envisioned softwarized multi-swarming uavs to tackle covid-i9 situations," *IEEE Network*, pp. 1–8, 2020.

[5] A. Fotouhi, H. Qiang, M. Ding, M. Hassan, L. G. Giordano, A. Garcia-Rodriguez, and J. Yuan, "Survey on UAV Cellular Communications: Practical Aspects, Standardization Advancements, Regulation, and Security Challenges," *in IEEE Communications Surveys Tutorials*, vol. 21, no. 4, pp. 3417–3442, Fourthquarter 2019.

[6] X. Wang, H. Zhang, Y. Tian, and V. C. M. Leung, "Modeling and Analysis of Aerial Base Station-Assisted Cellular Networks in Finite Areas Under LoS and NLoS Propagation," *in IEEE Transactions on Wireless Communications*, vol. 17, no. 10, pp. 6985–7000, Oct 2018.

[7] 3GPP Technical Report 22.829. Technical specification group radio access network; Enhancement for Unmanned Aerial Vehicles; Stage 1 (Release 17), Sept. 2019.

[8] Y. Zeng, R. Zhang, and T. J. Lim, "Wireless communications with unmanned aerial vehicles: opportunities and challenges," *in IEEE Communications Magazine*, vol. 54, no. 5, pp. 36–42, May 2016.

[9] B. Bera, S. Saha, A. K. Das, N. Kumar, P. Lorenz, and M. Alazab, "Blockchain-envisioned secure data delivery and collection scheme for 5g-based iot-enabled internet of drones environment," *IEEE Transactions on Vehicular Technology*, vol. 69, no. 8, pp. 9097–9111, 2020.

[10] A. A. Khuwaja, Y. Chen, N. Zhao, M. Alouini, and P. Dobbins, "A Survey of Channel Modeling for UAV Communications," *in IEEE Communications Surveys Tutorials*, pp. 1–1, 2018.

[11] C. Yan, L. Fu, J. Zhang, and J. Wang, "A Comprehensive Survey on UAV Communication Channel Modeling," *in IEEE Access*, vol. 7, pp. 107 769–107 792, 2019.

[12] W. Khawaja, I. Guvenc, D. W. Matolak, U. Fiebig, and N. Schneckenburger, "A Survey of Air-to-Ground Propagation Channel Modeling for Unmanned Aerial Vehicles," *in IEEE Communications Surveys Tutorials*, vol. 21, no. 3, pp. 2361–2391, thirdquarter 2019.

[13] N. Sharma, M. Magarini, L. Dossi, L. Reggiani, and R. Nebuloni, "A study of channel model parameters for aerial base stations at 2.4 GHz in different environments," in *15th IEEE Annual Consumer Communications Networking Conference (CCNC)*, Jan 2018, pp. 1–6.

[14] R. Zhang, Q. Guo, D. Zhai, D. Zhou, X. Du, and M. Guizani, "Channel Measurement and Resource Allocation Scheme for Dual-Band Airborne Access Networks," *in IEEE Access*, vol. 7, pp. 80 870–80 883, 2019.

[15] Z. Cui, C. Briso, K. Guan, D. W. Matolak, C. Calvo-Ramirez, B. Ai, and Z. Zhong, "Low-altitude UAV air-ground propagation channel measurement and analysis in a suburban environment at 3.9 GHz," *in IET Microwaves, Antennas Propagation*, vol. 13, no. 9, pp. 1503–1508, 2019.

[16] A. Al-Hourani, S. Kandeepan, and S. Lardner, "Optimal LAP Altitude for Maximum Coverage," *in IEEE Wireless Communications Letters*, vol. 3, no. 6, pp. 569–572, Dec 2014.

[17] M. M. Azari, F. Rosas, K. Chen, and S. Pollin, "Ultra Reliable UAV Communication Using Altitude and Cooperation Diversity," *in IEEE Transactions on Communications*, vol. 66, no. 1, pp. 330–344, Jan 2018.

[18] H. He, S. Zhang, Y. Zeng, and R. Zhang, "Joint Altitude and Beamwidth Optimization for UAV-Enabled Multiuser Communications," *in IEEE Communications Letters*, vol. 22, no. 2, pp. 344–347, Feb 2018.

[19] W. Huang, D. M. Kim, W. Ding, and P. Popovski, "Joint Optimization of Altitude and Transmission Direction in UAV-Based Two-Way Communication," *in IEEE Wireless Communications Letters*, vol. 8, no. 4, pp. 984–987, Aug 2019.

[20] K. Lim, H. Kim, T. C. Hong, and J. Y. Ahn, "Wideband channel waveform and structure for unmanned aircraft systems," in *International Conference on Information and Communication Technology Convergence (ICTC)*, Oct 2017, pp. 1222–1224.

[21] J. Kakar and V. Marojevic, "Waveform and spectrum management for unmanned aerial systems beyond 2025," in *IEEE 28th Annual International Symposium on Personal, Indoor, and Mobile Radio Communications (PIMRC)*, Oct 2017, pp. 1–5.

[22] Z. Wu, H. Kumar, and A. Davari, "Performance evaluation of OFDM transmission in UAV wireless communication," in *Proceedings of the Thirty-Seventh Southeastern Symposium on System Theory, 2005. SSST '05.*, March 2005, pp. 6–10.

[23] M. Jacovic, O. Bshara, and K. R. Dandekar, "Waveform Design of UAV Data Links in Urban Environments for Interference Mitigation," in *IEEE 88th Vehicular Technology Conference (VTC-Fall)*, Aug 2018, pp. 1–5.

[24] C. Blümm, C. Heller, and R. Weigel, "SDR OFDM waveform design for a UGV/UAV communication scenario," *in Journal of Signal Processing Systems*, vol. 69, no. 1, pp. 11–21, 2012.

[25] Y. Yang, L. Zhu, X. Mao, Q. Tan, and Z. He, "The spread spectrum GFDM schemes for integrated satellite-terrestrial communication system," *China Communications*, vol. 16, no. 12, pp. 165–175, 2019.

[26] M. Murad, I. A. Tasadduq, and P. Otero, "Towards multicarrier waveforms beyond OFDM: Performance analysis of GFDM modulation for underwater acoustic channels," *IEEE Access*, pp. 1–1, 2020.

[27] K. Vejandla, S. P. Valluri, V. M. V, S. Mathini, A. Kumar, and T. Ratnarajah, "Performance Analysis Under Double Sided Clipping and Real Time Implementation of DCO-GFDM in VLC Systems," *Journal of Lightwave Technology*, pp. 1–1, 2020.

[28] Z. Na, J. Lv, F. Jiang, M. Xiong, and N. Zhao, "Joint Subcarrier and Subsymbol Allocation-Based Simultaneous Wireless Information and Power Transfer for Multiuser GFDM in IoT," *IEEE Internet of Things Journal*, vol. 6, no. 4, pp. 5999–6006, 2019.

[29] Qualcomm, "Cellular Drone Communication". URL:https://www.qualcomm.com/invention/technologies/lte/advanced-pro/cellular-drone-communication.

[30] Facebook, "The technology behind Aquila". URL:https://www.facebook.com/notes/mark-zuckerberg/the-technology-behind-aquila/10153916136506634/.

[31] Nokia, "Connected UAVs". URL:https://networks.nokia.com/products/ConnectedUAVs.

[32] I. Gaspar, L. Mendes, M. Matthé, N. Michailow, A. Festag, and G. Fettweis, "LTE-compatible 5G PHY based on generalized frequency division multiplexing," in *11th International Symposium on Wireless Communications Systems (ISWCS)*, Aug 2014, pp. 209–213.

[33] R. Blasco, H. Do, S. Shalmashi, S. Sorrentino, and Y. Zang, "3gpp lte enhancements for v2v and comparison to ieee 802.11 p," in *11th ITS European Congress, no. EU-SP0264*, 2016, pp. 6–9.

[34] A. Festag, "Cooperative intelligent transport systems standards in europe," *IEEE Communications Magazine*, vol. 52, no. 12, pp. 166–172, 2014.

[35] D. Zhang, A. Festag, and G. P. Fettweis, "Performance of generalized frequency division multiplexing based physical layer in vehicular communications," *IEEE Transactions on Vehicular Technology*, vol. 66, no. 11, pp. 9809–9824, 2017.

[36] N. Michailow, M. Matthé, I. S. Gaspar, A. N. Caldevilla, L. L. Mendes, A. Festag, and G. Fettweis, "Generalized Frequency Division Multiplexing for 5th Generation Cellular Networks," *in IEEE Transactions on Communications*, vol. 62, no. 9, pp. 3045–3061, Sept 2014.

[37] W. Khawaja, I. Guvenc, D. Matolak, U.-C. Fiebig, and N. Schneckenberger, "A Survey of Air-to-Ground Propagation Channel Modeling for Unmanned Aerial Vehicles," *in ArXiv e-prints*, Jan. 2018.

[38] A. Kumar, M. Magarini, and S. Bregni, "Impact of Better than Nyquist pulse shaping in GFDM PHY with LTE-compatible frame structure," in *IEEE 9th Latin-American Conference on Communications (LATINCOM)*, Nov 2017, pp. 1–6.

[39] A. Kumar and M. Magarini, "Improved Nyquist pulse shaping filters for generalized frequency division multiplexing," in *8th IEEE Latin-American Conference on Communications (LATINCOM)*, Nov 2016, pp. 1–7.

[40] "Propagation data and prediction methods for the design of terrestrial broadband millimetric radio access systems," in *in Geneva, Switzerland, Rec. P.1410-2, 2003, P Series, Radiowave Propagation*.

[41] Wireless Insite, 3D Wireless Prediction Software. URL:https://www.remcom.com/wireless-insite-em-propagation-software/.

[42] P. Medeđović, M. Veletić, and Ž. Blagojević, "Wireless insite software verification via analysis and comparison of simulation and measurement results," in *MIPRO, 2012 Proceedings of the 35th International Convention*. IEEE, 2012, pp. 776–781.

[43] D. G. Cileo, N. Sharma, and M. Magarini, "Coverage, capacity and interference analysis for an aerial base station in different environments," in *International Symposium on Wireless Communication Systems (ISWCS)*, Aug 2017, pp. 281–286.

[44] S. Sun, T. S. Rappaport, S. Rangan, T. A. Thomas, A. Ghosh, I. Z. Kovacs, I. Rodriguez, O. Koymen, A. Partyka, and J. Jarvelainen, "Propagation Path Loss Models for 5G Urban Micro- and Macro-Cellular Scenarios," in *IEEE 83rd Vehicular Technology Conference (VTC Spring)*, May 2016, pp. 1–6.

[45] "Solid Angle" From MathWorld–A Wolfram Web Resource. URL:http://mathworld.wolfram.com/SolidAngle.html.

[46] C. C. Tan and N. C. Beaulieu, "An investigation of transmission properties of Xia pulses," in *IEEE International Conference on Communications (Cat. No. 99CH36311)*, vol. 2, 1999, pp. 1197–1201 vol.2.

**Navuday Sharma** received his M-Tech in avionics engineering from Institute of Space Science and Technology, Amity University, Uttar Pradesh, India, in 2015 and Ph.D. degree in telecommunication engineering from the Department of Electronics, Information and Bio-engineering (DEIB), Politecnico di Milano, Italy, in 2018. He was also a Research Engineer at Infocomm Lab, School of Computer Science and Robotics, Tomsk Polytechnic University, Russia, from Oct 2017 to June 2018. Further, he has worked as a Post-Doctoral Researcher at Thomas Johann Seebeck Department of Electronics, Tallinn University of Technology, Estonia from Oct 2018 to Feb 2020. Currently, he is a RF Test Development Engineer at Ericsson Estonia. He has worked on wireless communication with aerial base stations for 5G systems and currently working towards ultra-reliable low latency communication. His other research interests are channel modeling, multi-carrier communication, digital signal processing and internet of things.

**Atul Kumar** received the B.Tech. degree in electronics and communication engineering, in 2013, and the M.S. degree in electronics engineering in September 2015, and Ph.D. degree in information engineering at the Dipartimento di Elettronica, Informazione and Bioingegneria in December 2018 from the Politecnico di Milano, Milan, Italy. Currently he is research associate in Vodafone Chair Mobile Communications Systems, Technische Universität Dresden, Germany from December 2018. His main research interests include wireless cellular systems, synchronization errors, LTE-A Physical layers, New Radio, Beam forming, massive multiple-input and multiple-output, orthogonal frequency division multiplexing, generalized frequency division multiplexing, and non-orthogonal multiple access.

**Haris Pervaiz** received the M.Sc. degree in information security from the Royal Holloway University of London, Egham, U.K., in 2005, and the Ph.D. degree from the School of Computing and Communication, Lancaster University, Lancaster, U.K., in 2016, where he is currently working as a lecturer with InfoLab21. He was a research fellow with the 5G Innovation Centre, University of Surrey, Guildford, U.K., from 2017 to 2018, and an EPSRC Doctoral Prize Fellow with the School of Computing and Communication, Lancaster University, from 2016 to 2017. His current research interests include green heterogeneous wireless communications and networking, 5G and beyond, millimeter wave communication, and energy and spectral efficiency. He has been actively involved in projects, such as CROWN, CogGREEN, TWEETHER, and Energy Proportional EnodeB for LTE-Advanced and Beyond and the DARE project, and an ESPRC funded project. He is an associate editor of IEEE Access, an editorial board member of Emerging Telecommunications Technologies (Wiley), and an associate editor of Internet Technology Letters (Wiley).

**Maurizio Magarini** received the M.Sc. and Ph.D. degrees in electronic engineering from the Politecnico di Milano, Milan, Italy, in 1994 and 1999, respectively. In 1994, he was granted the TELECOM Italia scholarship award for his M.Sc. Thesis. He worked as a Research Associate in the Dipartimento di Elettronica, Informazione e Bioingegneria at the Politecnico di Milano from 1999 to 2001. From 2001 to 2018, he was an Assistant Professor in Politecnico di Milano where, since June 2018, he has been an Associate Professor. From August 2008 to January 2009 he spent a sabbatical leave at Bell Labs, Alcatel-Lucent, Holmdel, NJ. His research interests are in the broad area of communication and information theory. Topics include synchronization, channel estimation, equalization and coding applied to wireless and optical communication systems. His most recent research activities have focused on molecular communications, massive MIMO, study of waveforms for 5G cellular systems, vehicular communications, wireless sensor networks for mission critical applications, and wireless networks using unmanned aerial vehicles and high-altitude platforms. He has authored and coauthored more than 100 journal and conference papers. He was the co-recipient of two best-paper awards. He is an Associate Editor of IEEE Access, IET Electronics Letters, and Nano Communication Networks (Elsevier). He has been involved in several European and National research projects.

**Leila Musavian** received her PhD degree in Telecommunications from Kings College London, UK. She is currently working as Professor of Wireless Communications at University of Essex. She was Deputy Pro-Vice-Chancellor for Research at University of Essex between September 2018 and December 2020 and Reader in Telecommunications at the School of Computer Science and Electronic Engineering from Dec 2016-Oct 2020. Prior to that, she was Lecturer at InfoLab21, Lancaster University (Dec 2012-Aug 2016), Senior Lecturer at InfoLab21, Lancaster University (Aug 2016-Nov 2016), Research Associate at McGill University (2011-2012), research associate at Loughborough University, UK (2009-2010) and post-doctoral fellow at INRS-EMT, Canada (2006-2008). Her research interests lie in Radio Resource Management for 6G/B5G communications, low latency communications, Machine learning for Communications, mmWave Communications, Massive MIMO and Energy Harvesting Communications.

She has been editor of IEEE TRANSACTIONS OF WIRELESS COMMUNICATIONS between 2015-2020. She was Executive Editor of Transactions on Emerging Telecommunications Technologies between 2016-2019 and Associate Editor of Wiley's Internet Technology Letters. She has been lead chair for UHS5G WP in IEEE Globecom 2018, UHSLLS WP in IEEE WCNC 2019, lead chair for URLLC Special Session in IEEE PIMRC 2018, TPC Co-Chair of CorNer 2016 (in conjunction with ISWCS 2016) and Co-Chair of mmWave 5G (STEMCOM 2016) and also TPC member of several conferences including IEEE ICC, IEEE GLOBECOM, IEEE WCNC, IEEE ICCCN, IEEE PIMRC, ChinaCom, etc. She was the workshop co-chair of VTC-Spring-2020 and is currently the Wireless Communications Symposium Lead Co-Chair for IEEE ICC 2021, in Montreal, Canada.

**Muhamamd Mahtab Alam** (M'07, SM'19) received M.Sc. degree in electrical engineering from Aalborg University, Denmark, in 2007, and Ph.D. degree in signal processing and telecommunication from the University of Rennes1 France (INRIA Research Center) in 2013. He joined Swedish College of Engineering and Technology, Pakistan, in 2013 as assistant professor. He did his postdoc research from 2014-2016 at Qatar Mobility Innovation Center, Qatar. In 2016, he joined as European Research Area Chair and Associate Professor at Thomas Johann Seebeck Department of Electronics at Tallinn University of Technology, where later in 2018 he was elected as Professor. From 2019, he is the communication systems research group leader. His research focusses on the fields of wireless communications - connectivity, NB-IoT 5G/B5G services and applications, low-power wearable networks for SmartHealth. He has15+ years of combined academic and industrial multinational experiences while working in Denmark, Belgium, France, Qatar and Estonia. He has several leading roles as PI in multimillion Euros international projects funded by European Commission (H2020-ICT-2019-3, "951867", NATO-SPS (G5482), Estonian Research Council (PRG424), Telia industrial grant etc. He is author and co-author of more than 85 research publications.

**Anish Jindal** (M'16, SM'17) is working as a Lecturer in School of Computer Science and Electronic Engineering (CSEE), University of Essex since Mar 2020. Prior to this, he worked as senior research associate at School of Computing Communications, Lancaster University, UK from Oct. 2018 to Mar. 2020. He completed his Ph.D., M.E. and B. Tech. degrees in computer science engineering in 2018, 2014, and 2012, respectively. He is the recipient of the Outstanding Ph.D. Dissertation Award, 2019 from IEEE Technical Committee on Scalable Computing (TCSC) and conferred with the IEEE Communication Society's Outstanding Young Researcher Award for the Europe, Middle East, and Africa (EMEA) Region, 2019. He has served as General co-chair, TPC co-chair, TPC member, Publicity chair and Session chair of various reputed conferences and workshops including IEEE ICC, IEEE WoWMoM, IEEE INFOCOM and IEEE GLOBECOM. He is also the guest editor of various journals including Software: Practice and Experience (Wiley) and Computers (MDPI). His research interests are in the areas of smart cities, data analytics, artificial intelligence, cyber-physical systems, wireless networks, and security. He is a member of the IEEE and actively involved with various working groups and committees of IEEE and ACM related to smart grid, energy informatics and smart cities.

**Muhammad Ali Imran** (M'03, SM'12) Fellow IET, Senior Member IEEE, Senior Fellow HEA is Dean University of Glasgow UESTC and a Professor of Wireless Communication Systems with research interests in self organised networks, wireless networked control systems and the wireless sensor systems. He heads the Communications, Sensing and Imaging (CSI) research group at University of Glasgow and is Director of Centre for Educational Development and Innovation. He is an Affiliate Professor at the University of Oklahoma, USA and a visiting Professor at 5G Innovation Centre, University of Surrey, UK. He has over 20 years of combined academic and industry experience with several leading roles in multi-million pounds funded projects. He has filed 15 patents; has authored/co-authored over 400 journal and conference publications; has authored 2 books, edited 8 books and authored more than 30 book chapters; has successfully supervised over 40 postgraduate students at Doctoral level. He has been a consultant to international projects and local companies in the area of self-organised networks.